Three-Dimensional Structure of Phosphotriesterase: An Enzyme Capable of Detoxifying Organophosphate Nerve Agents[†,‡]

Matthew M. Benning,*[,§] Jane M. Kuo,[||] Frank M. Raushel,[||] and Hazel M. Holden[§]

Department of Biochemistry and the Institute for Enzyme Research, University of Wisconsin, 1710 University Avenue, Madison, Wisconsin 53705, and Department of Chemistry, Texas A&M University, College Station, Texas 77843

Received July 21, 1994; Revised Manuscript Received September 7, 1994[⊗]

ABSTRACT: Organophosphates, such as parathion and paraoxon, constitute the largest class of insecticides currently used in industrialized nations. In addition, many of these compounds are known to inhibit mammalian acetylcholinesterases thereby acting as nerve agents. Consequently, organophosphate-degrading enzymes are of considerable interest in light of their ability to detoxify such compounds. Here we report the three-dimensional structure of such an enzyme, namely, phosphotriesterase, as determined by single crystal X-ray diffraction analysis to 2.1-Å resolution. Crystals employed in this investigation belonged to the space group $P2_12_12$ with unit cell dimensions of $a = 80.3$ Å, $b = 93.4$ Å, and $c = 44.8$ Å and one molecule per asymmetric unit. The structure was solved by multiple isomorphous replacement with two heavy-atom derivatives and refined to a crystallographic R factor of 18.0%. As observed in various other enzymes, the overall fold of the molecule consists of an α/β barrel with eight strands of parallel β-pleated sheet. In addition, there are two antiparallel β-strands at the N-terminus. The molecular model of phosphotriesterase presented here provides the initial structural framework necessary toward understanding the enzyme's broad substrate specificities and its catalytic mechanism.

The phosphotriesterase from *Pseudomonas diminuta* catalyzes the hydrolysis of paraoxon and related acetylcholinesterase inhibitors with rate enhancements that approach 10^{12} (Dumas *et al.,* 1989). As a result, the enzyme has generated considerable interest for bioremediation applications due to the exhibited potential for the rapid and complete detoxification of organophosphate nerve agents such as sarin, soman, and various agricultural insecticides as shown in Figure 1 (Caldwell & Raushel, 1991). Although organophosphate triesters (and related phosphonates) are not naturally occurring materials, the turnover number (k_{cat}) of phosphotriesterase for the hydrolysis of paraoxon is nearly 10^4 s^{-1} (Omburo *et al.,* 1992), a value that exceeds the k_{cat} observed for most other enzymes. The active site of phosphotriesterase is composed primarily of a binuclear metal center of undefined structure that is required for catalysis. The specific roles of the two metal ions and the other amino acid residues involved in the chemical mechanism are largely unknown (Omburo *et al.,* 1992). However, ^{113}Cd NMR (Omburo *et al.,* 1993) and Mn^{2+} EPR (Chae *et al.,* 1993) spectroscopy experiments, coupled with site-directed mutagenesis manipulations, have quite clearly indicated that the two required metal ions are bridged via a common ligand and that a majority of the other protein ligands to the binuclear metal cluster are imidazole side chains of histidine residues.

The evolution of an enzyme activity that is specific for the hydrolysis of organophosphate triesters is of interest since these compounds have existed as a distinct class of molecules for only a half century. Yet molecules such as paraoxon are hydrolyzed by this enzyme at the diffusion-controlled rate (Caldwell *et al.,* 1991), and thus far it has not been possible to detect catalytic activity with other examples of related functional groups that occur naturally. It is also of interest that the enzymes, as isolated from *P. diminuta* and *Flavobacterium sp.,* have identical protein and gene sequences (Mulbry & Karns, 1989). Amino acid sequence identity searches have failed to locate any primary homology

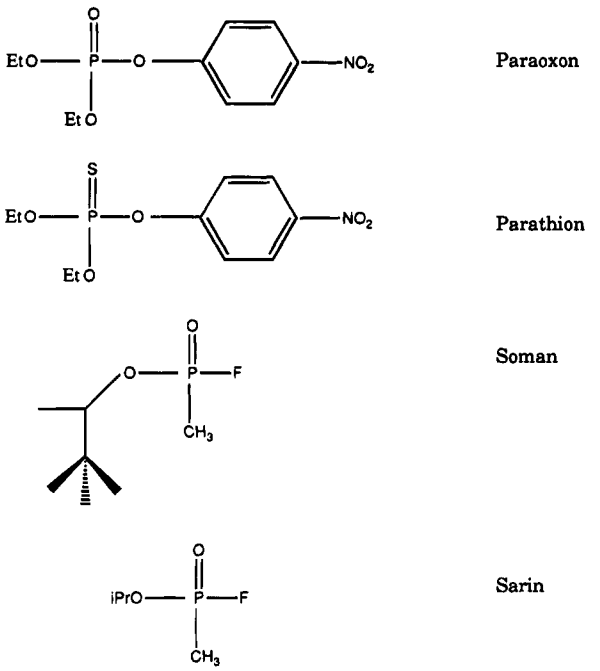

FIGURE 1: Organophosphate compounds susceptible to hydrolysis by phosphotriesterase. Paraoxon and parathion are typical insecticides, while soman and sarin are highly toxic inhibitors of mammalian acetylcholinesterases.

[†] This research was supported in part by grants from the NIH (GM-33894 to F.M.R. and DK47814 to H.M.H.) and the Naval Research Laboratory (N00014-91-K-2006 to F.M.R).

[‡] The coordinates have been deposited with the Brookhaven Protein Data Bank under filename 1PTA.

* To whom correspondence should be addressed.

[§] University of Wisconsin—Madison.

[||] Texas A&M University.

[⊗] Abstract published in *Advance ACS Abstracts,* November 15, 1994.

0006-2960/94/0433-15001$04.50/0

Table 1: Intensity Statistics for Native and Derivative Data

	resolution range (Å)							
	overall	100.00−4.00	3.17	2.77	2.52	2.34	2.20	2.09
native								
no. of measurements	93927	16377	15419	13288	11650	10826	10154	8985
no. of independent reflections	21816	3071	2936	2882	2781	2691	2662	2551
completeness of data (%)	93	99	99	98	96	93	92	88
average intensity	3459	10000	5853	2488	1286	904	664	457
average sigma	224	336	276	208	182	176	172	169
R factor (%)[a]	4.3	2.9	3.7	5.4	8.0	10.1	12.9	17.1
PHMPS								
no. of measurements	71525	18927	16284	13927	12036	8807	1540	0
no. of independent reflections	15022	3094	2947	2911	2816	2611	643	0
average intensity	5306	10000	6695	3212	1920	1358	929	0
average sigma	269	332	300	237	215	212	208	0
R factor (%)	3.68	2.9	3.4	4.9	6.7	8.4	11.1	0
trimethyllead acetate								
no. of measurements	48107	12664	11016	9293	8089	6039	1001	0
no. of independent reflections	13900	2970	2776	2714	2611	2260	569	0
average intensity	4731	10000	5662	2420	1289	825	669	0
average sigma	325	377	346	294	280	289	296	0
R factor (%)	4.0	2.8	3.7	6.5	10.3	14.6	18.0	0

[a] $R_{\text{factor}} = \sum|I - \bar{I}|/\sum I \times 100$.

Table 2: Refined Heavy Atom Parameters

derivative	site no.	relative occupancy	*x*	*y*	*z*	*B* (Å^2)[a]	R_{iso} (%)[b]	location
PHMPS	1	3.21	0.173	0.085	0.044	25.9	14.3	Cys 53
trimethyllead acetate	1	2.80	0.144	0.073	0.075	25.7	12.2	Cys 53, Glu 112

[a] Temperature factors were not refined. *x*, *y*, and *z* are the fractional atomic coordinates. [b] $R_{\text{iso}} = \sum|F_N - F_H|/\sum|F_N|$, where F_N is the native structure factor amplitude and F_H is the derivative structure factor amplitude.

with other enzymes. Here we describe the crystallization and X-ray structural determination of this bacterial phosphotriesterase.

MATERIALS AND METHODS

Crystallization and Preparation of Heavy-Atom Derivatives. The enzyme necessary for crystallization trials was purified according to published procedures and concentrated to 11 mg/mL (Omburo *et al.*, 1992). Protein samples contained 10 mM Hepes, pH 8.5. Single crystals were grown at room temperature by the hanging drop method of vapor diffusion. For these experiments, 5 μL of the protein solution was mixed with 5 μL of a solution containing 9% poly(ethylene glycol) 8000, 100 mM bicine (pH 9.0), 5 mM NaN_3, and 1 M LiCl. Crystals grew to typical dimensions of 0.5 mm × 0.5 mm × 0.2 mm.

For X-ray diffraction experiments, the crystals were mounted in quartz capillary tubes and cooled to 4 °C. By precession photography, the crystals were shown to belong to the space group $P2_12_12$ with unit cell dimensions of a = 80.3 Å, b = 93.4 Å, and c = 44.8 Å and one molecule per asymmetric unit.

Two heavy-atom derivatives were prepared by transferring the crystals first to a synthetic mother liquor containing 12% poly(ethylene glycol) 8000, 100 mM bicine, 1 M LiCl, and 5 mM NaN_3 and subsequently to solutions containing either 5 mM *p*-hydroxymercuriphenyl sulfonic acid or 5 mM trimethyllead acetate. Crystals were soaked in the mercury and lead-containing solutions for 22 and 19 h, respectively.

X-ray Data Collection and Processing. A native X-ray data set was collected to 2.0-Å resolution from a single crystal at 4 °C with a Siemens X1000D area detector system. The X-ray source was nickel-filtered Cu Kα radiation from a Rigaku RU200 X-ray generator operated at 50 kV and 50 mA and equipped with a 200 μm focal cup. A crystal-to-detector distance of 12 cm was used together with a step size of 0.15° per frame. The heavy-atom-derivative X-ray data sets were collected in a similar manner to 2.4-Å resolution. Friedel pairs were measured for all reflections in the heavy-atom-derivative data sets.

All X-ray data were processed with the data reduction software package XDS (Kabsch, 1988a,b) and internally scaled according to a procedure developed in the laboratory by Dr. Gary Wesenberg (G. Wesenberg and I. Rayment, manuscript in preparation). Relevant X-ray data collection statistics may be found in Table 1. The native X-ray data set was 93% complete to 2.0-Å resolution. The heavy-atom-derivative X-ray data sets were scaled to the native X-ray data in shells of equal volume in reciprocal space based on resolution.

The *R* factors between the native and the mercury and lead X-ray data sets were 14.3% and 12.2%, respectively, where

$$R \text{ factor} = (\sum||F_{\text{native}}| - |F_{\text{heavy-atom}}||/\sum|F_{\text{native}}|) \times 100$$

Structural Determination and Least-Squares Refinement. The positions of the heavy-atom-binding sites for the mercury and lead derivatives were determined by inspection of difference Patterson maps calculated with all X-ray data from 30- to 5-Å resolution. Each derivative contained only a single binding site. These sites were placed on a common origin by difference Fourier maps. The positions and occupancies of these sites were refined by the origin-removed

Table 3: Phase Calculation Statistics

	resolution range (Å)							
	∞−8.53	5.42	4.25	3.61	3.19	2.89	2.66	2.48
no. of reflections	699	1145	1453	1669	1892	2030	2178	2260
figure of merit	0.81	0.82	0.74	0.67	0.60	0.56	0.53	0.45
phasing power[a]								
PHMPS								
centric reflections	1.22	1.29	1.21	0.94	1.00	0.98	0.97	0.85
acentric reflections	1.76	1.72	1.49	1.35	1.29	1.37	1.38	1.20
trimethyllead acetate								
centric reflections	1.28	1.14	0.82	0.97	0.95	0.84	0.90	0.69
acentric reflections	1.62	1.56	1.15	1.22	1.25	1.24	1.14	0.97

[a] Phasing power is the ratio of the root-mean-square heavy-atom scattering factor amplitude to the root-mean-square lack of closure error.

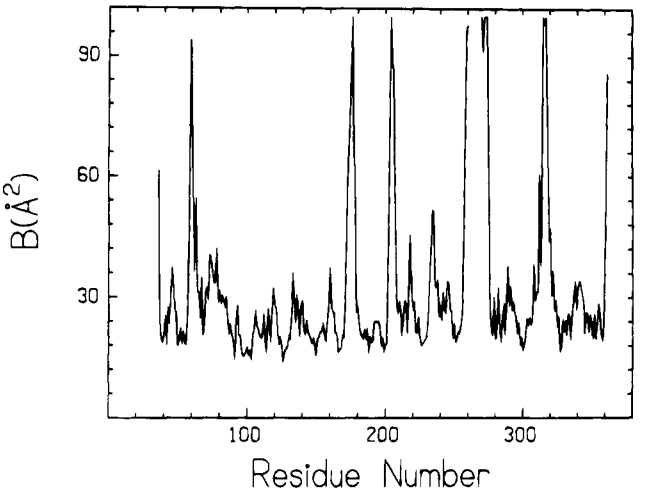

FIGURE 2: Plot of the mean main-chain temperature factors versus amino acid residue number. There is a break in the electron density such that residues Gly 261−Ser 269 are missing in the model. The first observable amino acid in the electron density map is Arg 36.

Patterson-function correlation method to 2.4-Å resolution and are listed in Table 2 (Rossmann, 1960; Terwilliger & Eisenberg, 1983). Since refinement of the thermal factors was not stable, these parameters were artificially set to a nominal value that gave a distribution of calculated heavy-atom differences consistent with the trend seen in the observed differences in the centric data. Anomalous difference Fourier maps calculated from 30- to 5 Å were employed for determining the correct hand of the heavy-atom constellation. Protein phases were calculated with the program HEAVY (Terwilliger & Eisenberg, 1983), and relevant phase calculation statistics may be found in Table 3.

An electron density map calculated to 2.4-Å resolution showed well-defined protein−solvent boundaries and clear regions of secondary structure. The map was further improved by the technique of solvent-flattening as implemented by Dr. W. Kabsch, Heidelberg, Germany (Wang, 1985). From this "density-modified" map it was possible to trace the polypeptide chain of phosphotriesterase from Arg 36 to Ile 260 and Ala 270 to Leu 362. The amino acid sequence employed for the fitting procedure was determined by Serder *et al.* (1989). Model building was accomplished with the program FRODO (Jones, 1985). Twelve cycles of alternate manual model building and least-squares refinement of the structure were conducted according to the method of Tronrud *et al.* (1987). Small peaks of electron density were considered to be water molecules if they were located within 3.5 Å of potential hydrogen-bonding groups. The average *B* value for the solvent was 41.2 Å^2. A plot of the mean main-chain temperature factors is shown in Figure 2. Phosphotriesterase contains 365 amino acid residues with the first 29 residues constituting a leader sequence (Mulbry & Karns, 1989). The protein utilized for this investigation starts at Ser 30 and terminates at Ser 365 (Kuo & Raushel, 1994). At the present stage of least-squares refinement there is no electron density prior to Arg 36 or following Leu 362. In addition, the surface loop defined by Gly 261 to Ser 269 is disordered and has not been included in the model. Relevant refinement statistics may be found in Table 4.

Table 4: Refinement Statistics

resolution limits (Å)	30.0−2.1
R factor (%)[a]	18.0
no. of reflections used	20330
no. of protein atoms	2439
no. of solvent atoms	129
weighted root-mean-square deviations from ideality	
bond length (Å)	0.014
bond angle (deg)	2.32
planarity (trigonal) (Å)	0.006
planarity (other planes) (Å)	0.012
torsional angle (deg)[b]	17.1

[a] R factor $= \Sigma|F_o - F_c|/\Sigma|F_o|$ where F_o is the observed structure-factor amplitude and F_c is the calculated structure-factor amplitude. [b] The torsional angles were not restrained during the refinement.

RESULTS AND DISCUSSION

Phosphotriesterase, as naturally isolated, contains up to 2 equiv of zinc per molecule. Catalytic activity is lost upon incubation of the protein with various chelating agents such as EDTA, 1,10-phenanthroline, and 8-hydroxyquinoline-5-sulfonic acid (Omburo *et al.*, 1992). The enzymatic activity of the protein can be restored by incubation with various divalent cations including Zn^{2+}, Co^{2+}, Ni^{2+}, Cd^{2+}, or Mn^{2+} (Omburo *et al.*, 1992). For the structural studies presented here, the apoenzyme was reconstituted with Cd^{2+} according to previously published procedures (Omburo *et al.*, 1992). Quite surprisingly, there were no large peaks in the electron density map corresponding to the bound cations although the protein employed for study was catalytically competent before the crystallization experiments. Most likely the crystallization solutions, which contained 100 mM bicine and 1 M LiCl at pH 9.0, effectively removed the metals from the enzyme. Consequently, the structure presented here is of the apo form. Initial attempts at soaking metals into the apo crystals have resulted in severe deterioration of their diffraction properties. Crystallization experiments of the holoenzyme with different buffers and salts are currently in progress.

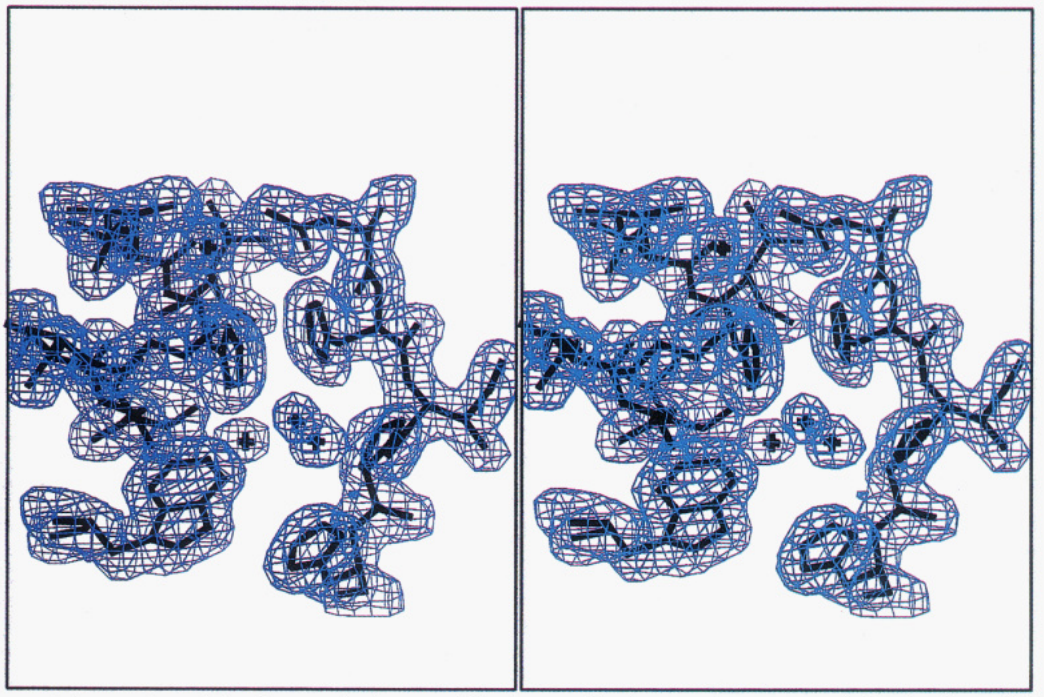

FIGURE 3: Representative portion of the electron density map. The electron density map shown was calculated with coefficients of the form $(2F_o - F_c)$ where F_o was the native structure factor amplitude and F_c was the calculated structure factor amplitude from the model refined at 2.1-Å resolution. Protein phases were calculated from the refined model. Small spheres of electron density correspond to ordered water molecules. The density on the right-hand side corresponds to Asp 253, His 254, Ile 255, Pro 256, and His 257. Electron density corresponding to Lys 169, His 201 and Trp 302 is shown on the left side. Note the close interaction between the N^{ζ} of Lys 169 and the imidazole ring of His 201.

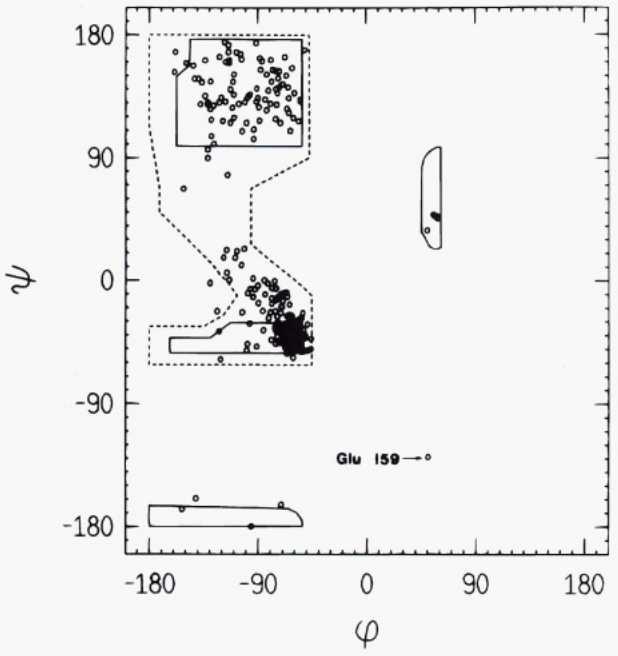

FIGURE 4: Ramachandran plot of the main-chain dihedral angles. Fully allowed ϕ,ψ values are enclosed by solid lines; those partially allowed are enclosed by dashed lines. The only outliers are Cys 59, Arg 96, Glu 159, Ala 203, and Asp 253.

A representative portion of the electron density map for phosphotriesterase is displayed in Figure 3. The electron density was well-ordered except for several residues located at the N- and C-termini and some situated in surface loops (Arg 36, Cys 59, Gly 60, Gly 174−Pro 178, Ala 203−Gln 206, Ser 258−Ile 274, Asp 315−Met 317, and Leu 362−Ser 365). As displayed in Figure 4, most of the non-glycinyl backbone dihedral angles were within the allowed regions of the Ramachandran plot except for Glu 159 which was located in a type II′ turn and adopted ϕ,ψ angles of 51.5° and −127.9°, respectively. This type of unfavorable interaction has been observed in various hydrolytic enzymes containing the α/β hydrolase fold (Ollis *et al.,* 1992). In these enzymes, it is the nucleophile of the so-called "catalytic triad" that adopts strained ϕ,ψ angles. In phosphotriesterase, however, Glu 159 is approximately 15 Å from the putative active site and most likely does not play a role in the catalytic mechanism. Rather, this residue is located within the subunit−subunit interface of the dimer as will be described below.

A ribbon representation of phosphotriesterase is displayed in Figure 5. The molecule is roughly globular with overall dimensions of approximately 51 Å × 55 Å × 51 Å. Its molecular architecture may be described simply as a distorted α/β barrel with eight parallel β-strands forming the barrel and flanked on the outer surface by 14 α-helices. In addition to this major tertiary structural element, there are two strands of antiparallel β-sheet at the N-terminus, 13 type I turns, one type I′ turn, two type II′ turns, and one helical turn. A list of the secondary structural elements is given in Table 5 with the β-strands labeled A−J. Two of the β-strands, namely, C and E, are disrupted by bulges formed by either His 55 ($\phi = 56°$, $\psi = 48°$) or Gly 129 ($\phi = 123°$, $\psi = -168°$), respectively. The α-helix formed by Gln 343−Leu 358 is also irregular due to Val 351, which adopts dihedral angles of $\phi = -121°$ and $\psi = -58°$.

While primary structural homology searches failed to detect similarities between phosphotriesterase and other proteins, this α/β-barrel motif has been observed in well over 20 enzymes. For an elegant discussion of the evolution of these enzymes, see Farber and Petsko (1990). The α/β-barrel enzymes represent an interesting and diverse structural family. In some cases, the α/β barrel constitutes most of

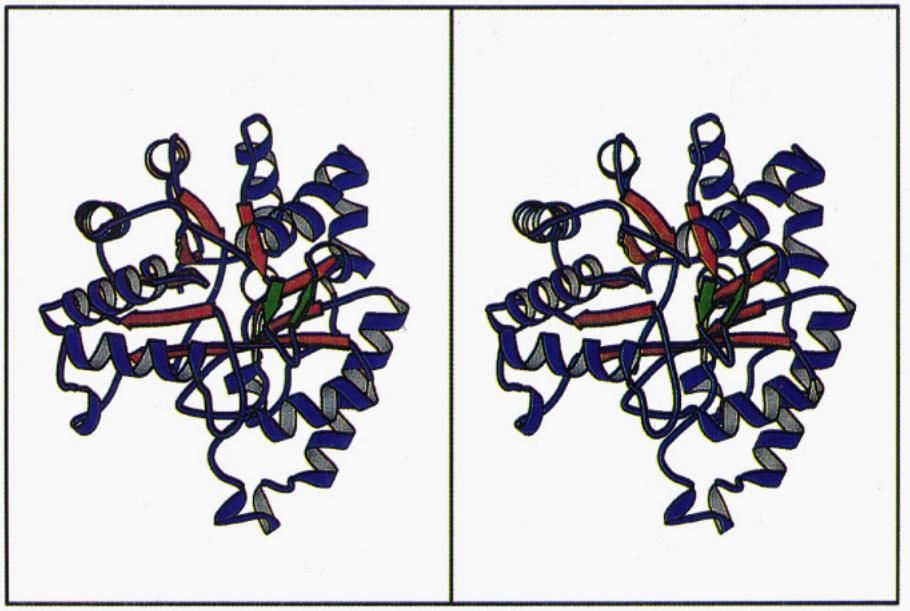

FIGURE 5: Ribbon representation of the phosphotriesterase. This figure was prepared with the program MOLSCRIPT (Kraulis, 1991). The first two β-strands are antiparallel and are displayed in green. The other eight β-strands, shown in red, form a distorted parallel β-barrel flanked on the sides by α-helices.

Table 5: List of Secondary Structural Elements

amino acid residues	type of structure	amino acid residues	type of structure
Arg 36−Asn 38	β-sheet (A)	Pro 197−His 201	β-sheet (G)
Thr 39−Gly 42	type I turn	Asp 208−Phe 216	α-helix
Pro 43−Thr 45	β-sheet (B)	Glu 217−Gly 220	~type I turn
Ile 46−Ala 49	α-helix	Ser 222−Arg 225	~type I turn
Phe 51−Glu 56	β-sheet (C)	Val 226−His 230	β-sheet (H)
Gly 60−Ala 63	type I turn	Leu 237−Leu 243	α-helix
Ser 62−Phe 65	type I′ turn	Ala 244−Gly 247	type I turn
Leu 66−Ala 68	helical turn	Leu 249−Leu 252	β-sheet (I)
Pro 70−Phe 73	α-helix	Trp 277−Leu 287	α-helix
Arg 76−Ala 93	α-helix	Ile 288−Gly 291	type I turn
Thr 97−Asp 100	β-sheet (D)	Tyr 292−Gln 295	type I turn
Phe 104−Gly 107	type I turn	Ile 296−Ser 299	β-sheet (J)
Val 110−Ser 117	α-helix	Asn 300−Phe 304	α-helix
Arg 118−Asp 121	type I turn	Ser 308−Val 310	α-helix
Val 122−Trp 131	β-sheet (E)	Thr 311−Met 314	type I turn
Leu 136−Met 138	α-helix	Asn 321−Gly 324	type I turn
Met 138−Arg 141	type I turn	Asp 323−Ala 326	type II′ turn
Val 143−Gln 155	α-helix	Phe 327−Leu 336	α-helix
Ile 158−Thr 161	type II′ turn	Arg 337−Gly 340	type I turn
Ile 167−Thr 173	β-sheet (F)	Gln 343−Leu 358	α-helix
Pro 178−Thr 194	α-helix		

the structure as is the case for phosphotriesterase and triose phosphate isomerase (Banner *et al.*, 1975). In others, for example in pyruvate kinase, the barrel is only one domain of a multidomain protein (Muirhead *et al.*, 1986; Larsen *et al.*, 1994). The range of reactions catalyzed by these various enzymes is as equally diverse as their tertiary structures. In addition, some of these enzymes bind cofactors such as FMN, some contain heme or [4Fe-4S] clusters, and some require Mg^{2+}, Ca^{2+}, or a combination of Mg^{2+} and K^+ for catalytic activity. Regardless of their domain structures or their requirements for cofactors, however, the active sites of these enzymes are always located at the C-terminal portions of the β-barrel. Consequently, this suggests that the active site of phosphotriesterase also should be located at the C-terminal portion of the barrel.

The reaction mechanism of phosphotriesterase has been examined thoroughly and shown to proceed with inversion of configuration about the phosphorus of the substrate (Lewis *et al.*, 1988). It is presently believed that the hydrolysis of phosphotriesters occurs via an S_N2 mechanism whereby an active site base of the protein abstracts a proton from a water molecule. This "activated" water serves as the nucleophile and directly attacks the electrophilic phosphorus of the substrate in a single in-line displacement reaction (Lewis *et al.*, 1988). Through the use of site-directed mutagenesis, it has been established that six of the seven histidine residues in phosphotriesterase are involved either directly in its catalytic mechanism or indirectly by ligating the zinc ions to the protein (Kuo & Raushel, 1994; Lai *et al.*, 1994). Not unexpectedly, these six histidines residues (His 55, His 57, His 201, His 230, His 254, and His 257) are clustered in the enzyme at the C-terminal portion of the β-barrel.

A close-up view of these residues is displayed in Figure 6. For the sake of clarity, only those amino acid residues that lie within 3.5 Å of the histidines are shown. As can be seen, there is a striking stacking interaction between the imidazole rings of His 201 and His 254. In addition, $N^{\delta 1}$ of His 254 lies at 2.5 Å from $O^{\delta 1}$ of Asp 253. This acidic residue, in turn, participates in an electrostatic interaction with the side chain of His 55 thus serving as a bridge between His 254 and His 55. There is a very close contact between His 201 and Lys 169 where N^{ζ} of the lysine side chain lies at 2.1 Å from $N^{\epsilon 2}$ of the histidine side chain. This region of the electron density map is unambiguous as can be seen in Figure 3. There are two aromatic residues, Trp 302 and Tyr 239, located within the vicinity of this "histidine cluster". The carbonyl oxygen of His 230 lies at 3.3 Å from $N^{\epsilon 1}$ of Trp 302 while $N^{\epsilon 2}$ of its imidazole side chain forms a hydrogen bond with the hydroxyl group of Tyr 239. Details concerning both the metal ligation and the active site base must await the structural determination of the holoenzyme. Most likely there are significant movements of the histidine residues upon formation of the holoenzyme, particularly with respect to His 201 and His 254, and such a rearrangement would contribute to the deterioration of the diffraction pattern of the crystals upon metal binding.

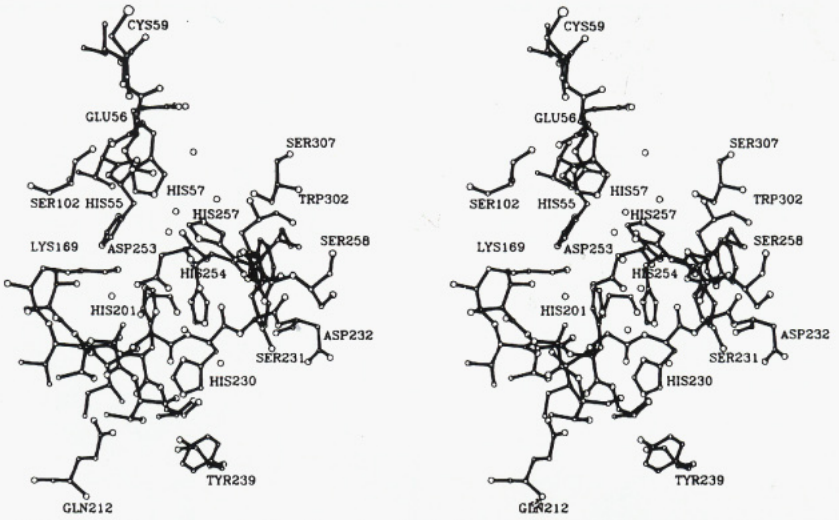

FIGURE 6: Close-up view of the "histidine cluster". For the sake of clarity only those amino acid residues within 3.5 Å of histidines 55, 57, 201, 230, 254, and 257 are shown. Again, for simplicity, only those residues that could possibly act as metal ligands or as active site bases are labeled. Those amino acids not labeled include Thr 54, Ile 58, Val 170, Ala 171, Thr 172, Thr 199, Thr 200, Thr 202, Ile 228, Gly 229, Gly 251, Ile 255, and Pro 256.

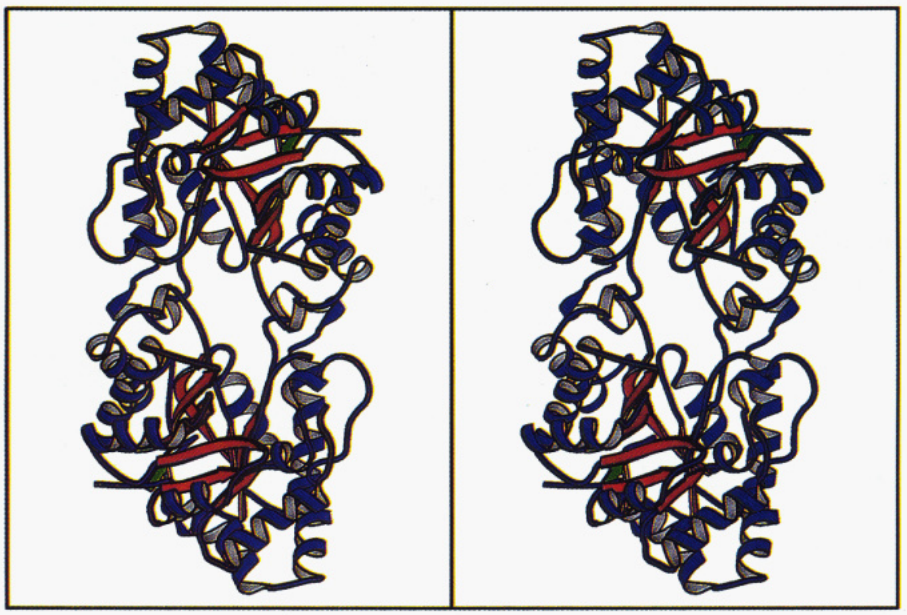

FIGURE 7: Ribbon representation of the phosphotriesterase dimer. The molecule is oriented such that the crystallographic 2-fold rotational axis is perpendicular to the plane of the page. There are extensive intermolecular interactions formed by the two surface loops delineated by Ser 61−Phe 73 and Asp 33−Arg 52 in subunits I and II, respectively. The overall dimensions of the dimer are approximately 61 Å × 86 Å × 51 Å.

Prior to the structural determination of phosphotriesterase described here, it was generally assumed that the enzyme functioned as a monomer. As the polypeptide chain was being traced, however, it became obvious that one extended surface loop, defined by Ser 61−Phe 73, made extensive contacts with a 2-fold-related molecule in the crystalline lattice. This loop contains four aromatic residues (Phe 65, Trp 69, Phe 72, and Phe 73) which participate in various stacking interactions. In particular, the aromatic ring of Phe 65 forms a stacking interaction with Met 138 and Phe 104 of the 2-fold-related molecule. Trp 69 is involved in two stacking interactions, one with Phe 149 in a symmetry-related molecule and the other with Phe 72 in the same molecule. The aromatic ring of Phe 72, in turn, lies perpendicular to that of Phe 73. Aside from these aromatic contacts, there are numerous electrostatic interactions occurring along the interface between these symmetry-related molecules. Both the hydrophobic and electrostatic interactions strongly suggest that, indeed, phosphotriesterase is a dimer that packed in the unit cell with its symmetry axis coincident to the crystallographic dyad running parallel to the z axis. Subsequent ultracentrifugation studies have demonstrated that phosphotriesterase behaves as a dimer. The quaternary structure of the enzyme is shown in Figure 7. The total surface area buried upon dimer formation is approximately 3200 Å^2 using a search probe radius of 1.4 Å (Lee & Richards, 1971). Approximately 11% of the monomer surface is buried upon dimer formation. The "histidine clusters" are approximately 25 Å apart in the dimer.

The three-dimensional model of phosphotriesterase described here provides a framework to more clearly define the chemical mechanism for phosphotriester hydrolysis and the structural basis for the evolution of its substantial catalytic activity. This enzyme is unique among the organophosphate-degrading enzymes, such as the paraoxonases and the DFPases, in that it is capable of hydrolyzing both widely

used pesticides and the phosphofluoridates, such as sarin, which constitute the major chemical warfare deterrents stockpiled by the United States. While a complete molecular understanding of the enzyme must await the structural determination of the holoenzyme, nonetheless the three-dimensional structure of the apoprotein provides clearer targets for continued site-directed mutagenesis investigations. Due to its ability to detoxify such a wide range of chemical agents and the fact that it can be produced in large quantities, the phosphotriesterase is an ideal candidate for applications designed to destroy organophosphate pesticides and mammalian acetylcholinesterase inhibitors. By a combination of site-directed mutagenesis experiments and structural studies, it may be possible in the future to design various enzymes with high specificities for sarin, soman, or other related compounds.

ACKNOWLEDGMENT

We thank Dr. Jim Remington for helpful discussions regarding the strained ϕ,ψ values observed in the α/β hydrolase enzymes and Dr. Grover L. Waldrop for critically reading the manuscript.

REFERENCES

Banner, D. W., Bloomer, A. C., Petsko, G. A., Phillips, D. C., Pogson, C. I., Wilson, I. A., Corran, P. H., Furth, A. J., Milman, J. D., Offord, R. E., Priddle, J. D., & Waley, S. G. (1975) *Nature 225*, 609−614.

Caldwell, S. R., & Raushel, F. M. (1991) *Appl. Biochem. Biotechnol. 31*, 59−73.

Caldwell, S. R., Newcomb, J. R., Schlecht, K. A., & Raushel, F. M. (1991) *Biochemistry 30*, 7438−7444.

Chae, M. Y., Omburo, G. A., Lindahl, P. A., & Raushel, F. M. (1993) *J. Am. Chem. Soc. 115*, 12173−12174.

Dumas, D. P., Caldwell, S. R., Wild, J. R., & Raushel, F. M. (1989) *J. Biol. Chem. 264*, 19659−19665.

Farber, G. K., & Petsko, G. A. (1990) *Trends Biochem. Sci. 15*, 228−234.

Jones, T. A. (1985) *Methods Enzymol.*, 157−171.

Kabsch, W. (1988a) *J. Appl. Crystallogr. 21*, 67−71.

Kabsch, W. (1988b) *J. Appl. Crystallogr. 21*, 916−924.

Kraulis, P. J. (1991) *J. Appl. Crystallogr. 24*, 946−950.

Kuo, J. M., & Raushel, F. M. (1994) *Biochemistry 33*, 4265−4272.

Lai, K., Dave, K. I., & Wild, J. R. (1994) *J. Biol. Chem.* (in press).

Larsen, T. M., Laughlin, T., Holden, H. M., Rayment, I., & Reed, G. H. (1994) *Biochemistry 33*, 6301−6309.

Lee, B., & Richards, F. M. (1971) *J. Mol. Biol. 55*, 379−400.

Lewis, V. E., Donarski, W. J., Wild, J. R., & Raushel, F. M. (1988) *Biochemistry 27*, 1591−1597.

Muirhead, H., Clayden, D. A., Barford, D., Lorimer, C. G., Fothergill-Gilmore, L. A., Schiltz, E., & Schmitt, W. (1986) *EMBO J. 5*, 475−481.

Mulbry, W. W., & Karns, J. S. (1989) *J. Bacteriol. 171*, 6740−6746.

Ollis, D. L., Cheah, E., Cygler, M., Dijkstra, B., Frolow, F., Franken, S. M., Harel, M., Remington, S. J., Silman, I., Schrag, J., Sussman, J. L., Verschueren , K. H. G., & Goldman, A. (1992) *Protein Eng. 5*, 197−211.

Omburo, G. A., Kuo, J. M., Mullins, L. S., & Raushel, F. M. (1992) *J. Biol. Chem. 267*, 13278−13283.

Omburo, G. A., Mullins, L. S., & Raushel, F. M. (1993) *Biochemistry 32*, 9148−9155.

Rossmann, M. G. (1960) *Acta Crystallogr. 13*, 221−226.

Serder, C. M., Murdock, D. C., & Rhode, M. F. (1989) *Bio/Technology 7*, 1151−1155.

Terwilliger, T. C., & Eisenberg, D. (1983) *Acta Crystallogr. Sect. A. 39*, 813−817.

Tronrud, D. E., Ten Eyck, L. F., & Matthews, B. W. (1987) *Acta Crystallogr. Sect. A. 43*, 489−501.

Wang, B. C. (1985) *Methods Enzymol. 115*, 90−112.